Calculations of the optical response of metallodielectric nanostructures of nonspherical particles by a layer-multiple-scattering method

N. Papanikolaou,[a] G. Gantzounis,[b] and N. Stefanou[b]

[a]Institute of Microelectronics, NCSR "Demokritos", Ag. Paraskevi, GR-153 10 Athens, Greece
[b]Section of Solid State Physics, University of Athens, Panepistimioupolis, GR-157 84 Athens, Greece

ABSTRACT

We present an efficient computational methodology for full electrodynamic calculations of metallodielectric nanostructures based on a multiple-scattering formulation of Maxwell's equations. The method, originally developed for systems of spherical particles (MULTEM code), is extended to systems of particles of arbitrary shape and applied to ordered structures of metallic nanodisks with an aspect ratio as large as five. We first discuss the particle plasmon resonances of single metallic nanocylinders of different aspect ratios. Then, we study the plasmonic excitations of square arrays of metal-dielectric-metal nanosandwiches and the optical response of a rectangular lattice of metallic nanodisks on a dielectric waveguide. Finally we analyse the photonic band structure of a simple cubic crystal of metallic nanodisks.

Keywords: Multiple scattering, plasmon, transmittance, nanodisk, nanosandwich, photonic band structure

1. INTRODUCTION

The optical properties of materials can be efficiently manipulated by periodic structuring on a length scale comparable to the wavelength of light. Recent advances in electron-beam lithography and self-assembly nanofabrication techniques allow one to prepare well-defined structures of nanoparticles with a tailored shape, size and arrangement, and observe new, interesting and potentially useful physical phenomena. In particular, considerable effort is devoted to the investigation of metallodielectric nanostructures, which open up impressive possibilities for tailoring the light-matter interaction. These are due, to a large extent, to the existence of plasmonic resonances in these systems, which can dramatically enhance the local electromagnetic (EM) field by concentrating EM energy into subwavelength volumes.[1,2]

Among the computational methodologies available for the study of the optical properties of metallodielectric systems containing periodic arrays of particles (scatterers) and homogeneous slabs, the so-called layer-multiple-scattering method has unique advantages.[3,4] Contrary to traditional band-structure or time-domain techniques, this method proceeds at a given frequency, i.e., it is an "on-shell" method and, therefore, it can be directly applied to structures made of strongly dispersive and absorptive materials such as real metals. Besides the complex band structure of a three-dimensional (3D) photonic crystal, associated with a given crystallographic plane, the method allows one to calculate, also, the transmission, reflection and absorption coefficients of an EM wave incident at a given angle on a finite slab of the crystal and, therefore, it can describe an actual transmission experiment. It is worthnoting that periodicity in the direction perpendicular to the layers is not required: the layers must only have the same two-dimensional (2D) periodicity. The layer-multiple-scattering method is proven very efficient for systems of spherical particles and, recently, an extension of the method to the treatment of nonspherical particles was formulated.[5] In the present work, we demonstrate the efficiency of this extended layer-multiple-scattering method on photonic systems of 2D and 3D ordered arrays of metallic nanodisks with an aspect ratio as large as 5. Such structures can be synthesized in the laboratory using modern nanofabrication techniques and attract considerable interest. In particular, we study the plasmonic excitations of square arrays

Further author information: (Send correspondence to N.P.)
N.P.: E-mail: N.Papanikolaou@imel.demokritos.gr, Telephone: +30 210 6503245

Nanophotonics II, edited by David L. Andrews, Jean-Michel Nunzi, Andreas Ostendorf,
Proc. of SPIE Vol. 6988, 69881D, (2008) · 0277-786X/08/$18 · doi: 10.1117/12.778844

of metal-dielectric-metal nanosandwiches, the optical response of a rectangular lattice of metallic nanodisks on a homogeneous dielectric waveguide and, finally, the complex photonic band structure of a simple cubic crystal of metallic nanodisks.

2. LIGHT SCATTERING BY A CYLINDRICAL METALLIC NANOPARTICLE

In the present work we shall be concerned with metallic nanoparticles, characterized by a (relative) magnetic permeability $\mu_{\rm s} = 1$ and a (relative) dielectric function $\epsilon_{\rm s}$. We assume, to begin with, that $\epsilon_{\rm s}$ has the simple yet effective Drude form[6]

$$\epsilon_{\rm s}(\omega) = 1 - \frac{\omega_{\rm p}^2}{\omega(\omega + {\rm i}\tau^{-1})} \ , \tag{1}$$

where $\omega_{\rm p}$ is the bulk plasma frequency and τ the relaxation time of the conduction-band electrons of the metal, which accounts for dissipative losses. When using the Drude dielectric function of Eq. (1), it is convenient to express the frequency in units of $\omega_{\rm p}$ and use $c/\omega_{\rm p}$ as the length unit, where c is the velocity of light in vacuum. We note that, considering a typical value 10 eV for $\hbar\omega_{\rm p}$, $c/\omega_{\rm p}$ corresponds to about 20 nm.

The scattering properties of a single particle can be obtained through the scattering T matrix. For the numerical evaluation of the elements of the T matrix for the particles under consideration, we employ the extended-boundary-condition method, properly adapted.[5] Truncating the relevant angular-momentum expansions at $\ell_{\rm max} = 12$, $\ell_{\rm cut} = 16$ and using a Gaussian quadrature integration formula with 4000 points for the integrals involved, our results have a relative error less than 10^{-3} in the considered range of frequencies.

The scattering T matrix is defined, in general terms, as the matrix which transforms the incident wave field, of amplitude $\mathbf{a}^0$ into the scattered wave field, of amplitude $\mathbf{a}^+$. In the basis of vector spherical waves we have

$$a^+_{P\ell m} = \sum_{P'\ell'm'} T_{P\ell m;P'\ell'm'} a^0_{P'\ell'm'} \ , \tag{2}$$

where $\ell = 1, 2, \ldots$ and $m = -\ell, -\ell+1, \ldots, \ell$ are the usual angular-momentum indices, and $P = E, H$ denotes the electric and magnetic multipole modes, respectively. For a spherical scatterer, $T_{P\ell m;P'\ell'm'} = T_{P\ell}\delta_{PP'}\delta_{\ell\ell'}\delta_{mm'}$. The causality condition implies that the eigenvalues of the T matrix are analytic functions in the upper complex frequency half-plane but they may have poles in the lower half-plane at $\omega_i - {\rm i}\gamma_i$, $\gamma_i \geq 0$; ω_i is the eigenfrequency while γ_i denotes the inverse of the lifetime of the respective mode. Among all possible solutions, resonant modes with $\gamma_i/\omega_i \ll 1$ are of particular physical interest. For example, a metallic nanosphere in a dielectric host medium exhibits such 2^ℓ-pole resonant modes of electric type at $\omega_\ell \simeq \omega_{\rm p}\sqrt{\ell/[\ell + (\ell+1)\epsilon]}$. These correspond to collective electron oscillations at the surface of the particle and are termed particle-plasmon modes. Similar plasmon modes also subsist in nonspherical particles but, in this case, $T_{P\ell m;P'\ell'm'}$ is no longer a diagonal matrix and thus there is no clear characterization of multipole modes. Nevertheless, for particles of cylindrical symmetry, the T matrix has a block-diagonal form and its eigenvalues are characterized by a given value of $|m|$ and a given parity, i.e., the corresponding eigenfields are either even or odd upon inversion.

In Fig. 1(a) we show the scattering cross section, normalized to the geometric cross section, for a single metallic nanodisk in air. The disk is described by the Drude dielectric function given by Eq. (1) without dissipative losses ($\tau^{-1} = 0$), and has a diameter $d \equiv 2S = 5c/\omega_{\rm p}$ and a thickness $h = c/\omega_{\rm p}$. In this case, obviously, the absorption cross section vanishes. An incoming plane wave is incident at an angle $\theta = 45^{\rm o}$ with respect to the disk axis (taken as the z axis) and is p-polarized, i.e., the electric field oscillates in the plane of incidence, which is defined by the disk axis and the direction of incidence. The excitation of several particle-plasmon modes is clearly visible in the figure. The peaks at $0.293\omega_{\rm p}$, $0.402\omega_{\rm p}$, and $0.465\omega_{\rm p}$ are associated with particle-plasmon modes corresponding to $m = \pm 1$, $m = \pm 2$, and $m = \pm 3$, respectively. All these modes are predominantly of electric type and have a mainly dipole, quadrupole, and octapole character, respectively.

Figure 1(b) depicts the corresponding results for a single metallic nanorod of diameter $d \equiv 2S = c/\omega_{\rm p}$ and length $L = 5c/\omega_{\rm p}$. In this case the observed resonances at $0.195\omega_{\rm p}$, $0.341\omega_{\rm p}$, and $0.438\omega_{\rm p}$ are associated with particle-plasmon modes corresponding to $m = 0$, predominantly of electric type, and have a mainly dipole, quadrupole, and again dipole character, respectively. It is interesting to note that the eigenfrequency of the fundamental mode, at $0.195\omega_{\rm p}$, is about 3 times smaller than that of an ideal half-wave dipole antenna ($L = \lambda/2$).

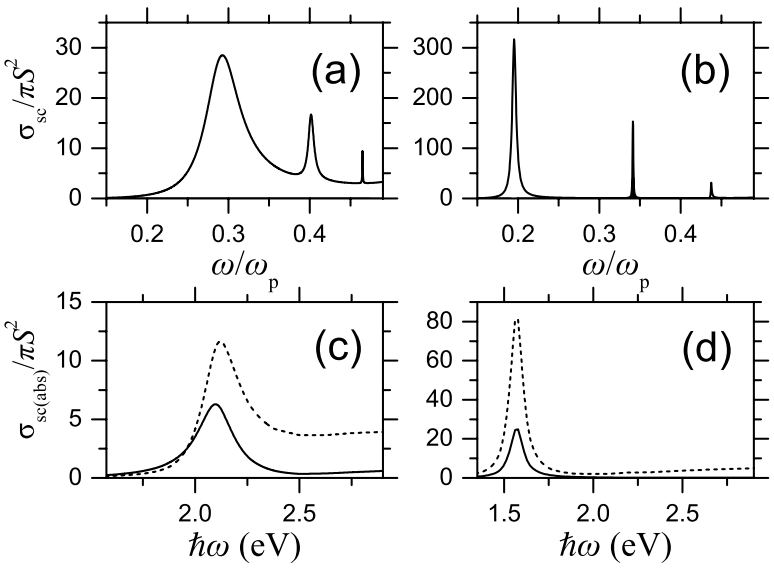

Figure 1. The scattering (solid lines) and absorption (dashed lines) cross sections of a gold nanodisk (left-hand diagrams) and a gold nanorod (right-hand diagrams) in air, for p-polarized light incident at an angle 45° with respect to the particle axis. In the upper diagrams the dielectric function of the particles, a disk of diameter $d \equiv 2S = 5c/\omega_p$ and thickness $h = c/\omega_p$ (a) and a rod of diameter $d \equiv 2S = c/\omega_p$ and length $L = 5c/\omega_p$ (b), is given by Eq. (1) with $\tau^{-1} = 0$, which implies that the absorption cross section is identically zero. In the lower diagrams the experimental dielectric function of bulk gold[7] is used for a disk of dimensions d =100 nm and h =20 nm (c) and a rod of dimensions d =20 nm and L =100 nm (d).

This is explained as follows. At optical frequencies the simple wavelength scaling $L = \lambda/2$ breaks down because incident radiation is no longer perfectly reflected from a metal's surface. Instead, the wave field penetrates into the metal and gives rise to surface-plasma oscillations. Hence, at optical frequencies an antenna does not respond to the external wavelength, λ, but to a shorter effective wavelength, $\lambda_{\rm eff}$, which depends on the material properties. Using the simple analytic approximation given by Novotny[8] for $\lambda_{\rm eff}$ in the case under consideration, we obtain a frequency $0.201\omega_p$, in very good agreement with our calculation ($0.195\omega_p$).

In Figs. 1(c), (d) we show the normalized scattering and absorption cross sections of an actual gold nanodisk, of dimensions d =100 nm, h =20 nm, and an actual gold nanorod, of dimensions d =20 nm, L =100 nm, respectively, in air. Here, for the dielectric function of gold we interpolate to the bulk values measured by Johnson and Christy[7] that include dissipative losses. It can be seen from the figure that, in the frequency region which interests us here, only the resonances associated with the fundamental particle-plasmon modes survive in each case. The higher modes are fully absorbed: they do not manifest themselves in the scattering cross section and appear as a broad background in the absorption cross section. This happens, obviously, because these modes have very long lifetimes as compared to the absorption time.

3. METALLODIELECTRIC NANOSTRUCTURES WITH A TWO-DIMENSIONAL PERIODICITY

We assume a plane of nonoverlapping particles, at $z = 0$, which are centered on the sites $\mathbf{R}_n$ of a given 2D lattice. Let a plane EM wave be incident on this layer. Because of the 2D periodicity of the structure under consideration, we write the component of the wave vector of the incident wave parallel to the layer, $\mathbf{q}_\parallel$, as $\mathbf{q}_\parallel = \mathbf{k}_\parallel + \mathbf{g}'$ where $\mathbf{k}_\parallel$, the reduced wave vector in the surface Brillouin zone (SBZ), is a conserved quantity in the scattering process

and $\mathbf{g}'$ is a certain reciprocal vector of the given lattice. Therefore, the wave vector of the incident wave has the form $\mathbf{K}^{\pm}_{\mathbf{g}'} = \mathbf{k}_{\parallel} + \mathbf{g}' \pm [q^2 - (\mathbf{k}_{\parallel} + \mathbf{g}')^2]^{1/2}\widehat{\mathbf{e}}_z$, where $\widehat{\mathbf{e}}_z$ is the unit vector along the z axis and the + or − sign refers to incidence from the left ($z < 0$) or from the right ($z > 0$). The corresponding electric field is written as

$$\mathbf{E}^{s'}_{\rm in}(\mathbf{r}) = [E_{\rm in}]^{s'}_{\mathbf{g}'i'} \exp(\mathrm{i}\mathbf{K}^{s'}_{\mathbf{g}'} \cdot \mathbf{r})\widehat{\mathbf{e}}_{i'} \ , \tag{3}$$

where $s' = +$ or $-$, and $i' = 1$ or 2 corresponds to a p- or s-polarized wave, $\widehat{\mathbf{e}}_1$, $\widehat{\mathbf{e}}_2$ being the polar and azimuthal unit vectors, respectively, which are perpendicular to $\mathbf{K}^{s'}_{\mathbf{g}'}$.

Since ω and $\mathbf{k}_{\parallel}$ are conserved quantities in the elastic scattering process, the scattered field will consist of a series of plane waves with wave vectors

$$\mathbf{K}^{\pm}_{\mathbf{g}} = \mathbf{k}_{\parallel} + \mathbf{g} \pm \left[q^2 - (\mathbf{k}_{\parallel} + \mathbf{g})^2\right]^{1/2} \widehat{\mathbf{e}}_z \ , \ \forall \mathbf{g} \tag{4}$$

and polarizations along $\widehat{\mathbf{e}}_1$ and $\widehat{\mathbf{e}}_2$ (polar and azimuthal unit vectors, respectively, associated with every $\mathbf{K}^s_{\mathbf{g}}$, $s = \pm$). Therefore we write

$$\mathbf{E}^s_{\rm sc}(\mathbf{r}) = \sum_{i=1}^{2} \sum_{\mathbf{g}} [E_{\rm sc}]^s_{\mathbf{g}i} \exp(\mathrm{i}\mathbf{K}^s_{\mathbf{g}} \cdot \mathbf{r})\widehat{\mathbf{e}}_i \ , \tag{5}$$

where the superscript $s = +(-)$ holds for $z > 0$ ($z < 0$). Though the scattered wave consists, in general, of a number of diffracted beams corresponding to different 2D reciprocal-lattice vectors $\mathbf{g}$, only beams for which $K^s_{\mathbf{g}z}$ is real constitute propagating waves. When $(\mathbf{k}_{\parallel} + \mathbf{g})^2 > q^2$ the corresponding wave decays to the right for $s = +$, and to the left for $s = -$; and the corresponding unit vectors $\widehat{\mathbf{e}}_i$ become complex but they are still orthonormal ($\widehat{\mathbf{e}}_i \cdot \widehat{\mathbf{e}}_j = \delta_{ij}$, $i, j = 1, 2$).

For example, when a plane wave is incident on the layer from the left, the transmitted wave (incident+scattered) on the right of the layer is given by

$$\mathbf{E}^+_{\rm tr}(\mathbf{r}) = \sum_{\mathbf{g}i} [E_{\rm tr}]^+_{\mathbf{g}i} \exp(\mathrm{i}\mathbf{K}^+_{\mathbf{g}} \cdot \mathbf{r})\widehat{\mathbf{e}}_i \ , \quad z > 0 \tag{6}$$

with $[E_{\rm tr}]^+_{\mathbf{g}i} = [E_{\rm in}]^+_{\mathbf{g}'i'}\delta_{\mathbf{g}\mathbf{g}'}\delta_{ii'} + [E_{\rm sc}]^+_{\mathbf{g}i} = S^{++}_{\mathbf{g}i;\mathbf{g}'i'}[E_{\rm in}]^+_{\mathbf{g}'i'}$ and the reflected wave on the left of the layer by

$$\mathbf{E}^-_{\rm rf}(\mathbf{r}) = \sum_{\mathbf{g}i} [E_{\rm rf}]^-_{\mathbf{g}i} \exp(\mathrm{i}\mathbf{K}^-_{\mathbf{g}} \cdot \mathbf{r})\widehat{\mathbf{e}}_i \ , \quad z < 0 \tag{7}$$

with $[E_{\rm rf}]^-_{\mathbf{g}i} = [E_{\rm sc}]^-_{\mathbf{g}i} = S^{-+}_{\mathbf{g}i;\mathbf{g}'i'}[E_{\rm in}]^+_{\mathbf{g}'i'}$. Similarly, we can define the transmission matrix elements $S^{--}_{\mathbf{g}i;\mathbf{g}'i'}$ and the reflection matrix elements $S^{+-}_{\mathbf{g}i;\mathbf{g}'i'}$ for a plane wave incident on the layer from the right. One can use the same notation (the calculation is of course much easier) to describe scattering by homogeneous layers: a homogeneous plate, or an interface between two homogeneous media. In these cases the S matrices are diagonal in $\mathbf{g}$ because of the translation invariance parallel to the xy plane. Explicit expressions for the matrix elements $S^{ss'}_{\mathbf{g}i;\mathbf{g}'i'}$, which obey the general symmetry relation: $S^{-s-s'}_{\mathbf{g}i;\mathbf{g}'i'} = (-1)^{i+i'} S^{ss'}_{\mathbf{g}i;\mathbf{g}'i'}$, are summarized elsewhere.[3,4]

In order to describe scattering by multilayers of particles with the same 2D periodicity, it is convenient to express the waves on the left of a given layer with respect to an origin, $\mathbf{A}_l$, on the left of the layer at $-\mathbf{d}_l$ from its center and the waves on the right of this layer with respect to an origin, $\mathbf{A}_r$, on the right of the layer at $\mathbf{d}_r$ from its center, i.e., a plane wave on the left of the layer will be written as $\mathbf{E}^s_{\mathbf{g}} \exp[\mathrm{i}\mathbf{K}^s_{\mathbf{g}} \cdot (\mathbf{r} - \mathbf{A}_l)]$ and a plane wave on the right of the layer will be written as $\mathbf{E}^s_{\mathbf{g}} \exp[\mathrm{i}\mathbf{K}^s_{\mathbf{g}} \cdot (\mathbf{r} - \mathbf{A}_r)]$. With the above choice of origins the transmission/reflection matrix elements of a layer become

$$\begin{aligned}
Q^{\rm I}_{\mathbf{g}i;\mathbf{g}';i'} &= S^{++}_{\mathbf{g}i;\mathbf{g}'i'} \exp\left[\mathrm{i}(\mathbf{K}^+_{\mathbf{g}} \cdot \mathbf{d}_r + \mathbf{K}^+_{\mathbf{g}'} \cdot \mathbf{d}_l)\right] \\
Q^{\rm II}_{\mathbf{g}i;\mathbf{g}';i'} &= S^{+-}_{\mathbf{g}i;\mathbf{g}'i'} \exp\left[\mathrm{i}(\mathbf{K}^+_{\mathbf{g}} \cdot \mathbf{d}_r - \mathbf{K}^-_{\mathbf{g}'} \cdot \mathbf{d}_r)\right] \\
Q^{\rm III}_{\mathbf{g}i;\mathbf{g}';i'} &= S^{-+}_{\mathbf{g}i;\mathbf{g}'i'} \exp\left[-\mathrm{i}(\mathbf{K}^-_{\mathbf{g}} \cdot \mathbf{d}_l - \mathbf{K}^+_{\mathbf{g}'} \cdot \mathbf{d}_l)\right] \\
Q^{\rm IV}_{\mathbf{g}i;\mathbf{g}';i'} &= S^{++}_{\mathbf{g}i;\mathbf{g}'i'} \exp\left[-\mathrm{i}(\mathbf{K}^-_{\mathbf{g}} \cdot \mathbf{d}_l + \mathbf{K}^-_{\mathbf{g}'} \cdot \mathbf{d}_r)\right] \ .
\end{aligned} \tag{8}$$

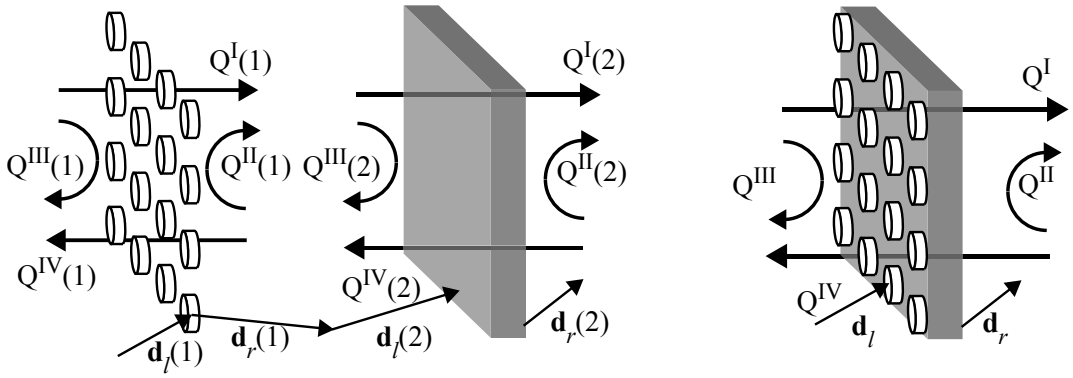

Figure 2. The Q matrices for two successive layers (right) are obtained from those of the individual layers (left).

The physical meaning of the Q-matrix elements is made obvious by their one-to-one correspondence with the S-matrix elements. In what follows the above matrices are written in compact form as $\mathbf{Q}^{\mathrm{I}}$, $\mathbf{Q}^{\mathrm{II}}$, $\mathbf{Q}^{\mathrm{III}}$ and $\mathbf{Q}^{\mathrm{IV}}$.

We obtain the transmission and reflection matrices for a pair of two successive layers, say "1" and "2" to be denoted by $\mathbf{Q}$, by combining the matrices $\mathbf{Q}(1)$ and $\mathbf{Q}(2)$ of the two layers, as shown schematically in Fig. 2. One can easily show that

$$\begin{aligned}
\mathbf{Q}^{\mathrm{I}} &= \mathbf{Q}^{\mathrm{I}}(2)\left[\mathbf{I}-\mathbf{Q}^{\mathrm{II}}(1)\mathbf{Q}^{\mathrm{III}}(2)\right]^{-1}\mathbf{Q}^{\mathrm{I}}(1)\\
\mathbf{Q}^{\mathrm{II}} &= \mathbf{Q}^{\mathrm{II}}(2)+\mathbf{Q}^{\mathrm{I}}(2)\mathbf{Q}^{\mathrm{II}}(1)\left[\mathbf{I}-\mathbf{Q}^{\mathrm{III}}(2)\mathbf{Q}^{\mathrm{II}}(1)\right]^{-1}\mathbf{Q}^{\mathrm{IV}}(2)\\
\mathbf{Q}^{\mathrm{III}} &= \mathbf{Q}^{\mathrm{III}}(1)+\mathbf{Q}^{\mathrm{IV}}(1)\mathbf{Q}^{\mathrm{III}}(2)\left[\mathbf{I}-\mathbf{Q}^{\mathrm{II}}(1)\mathbf{Q}^{\mathrm{III}}(2)\right]^{-1}\mathbf{Q}^{\mathrm{I}}(1)\\
\mathbf{Q}^{\mathrm{IV}} &= \mathbf{Q}^{\mathrm{IV}}(1)\left[\mathbf{I}-\mathbf{Q}^{\mathrm{III}}(2)\mathbf{Q}^{\mathrm{II}}(1)\right]^{-1}\mathbf{Q}^{\mathrm{IV}}(2)\,.
\end{aligned} \tag{9}$$

All matrices refer of course to the same ω and $\mathbf{k}_{\|}$; and we remember that the waves on the left and on the right of the pair of layers are referred to an origin at $-\mathbf{d}_l=-\mathbf{d}_l(1)$ from the center of the left layer and to an origin at $\mathbf{d}_r=\mathbf{d}_r(2)$ from the center of the right layer, respectively, as shown schematically in Fig. 2.

It is obvious that by the same process we can obtain the Q matrices of three layers, by combining those of the pair of layers with those of the third layer; and that we can similarly obtain the Q matrices for a slab consisting of any finite number of layers. When the layers making up the slab are the same, a most convenient way to obtain the Q matrices of the slab is provided by a doubling-layer scheme, whereby one obtains in sequence the Q matrices of a slab of $2, 4, 8, 16$ layers and so on, doubling at each stage the number of layers of the slab. Therefore, for a plane wave $[E_{\mathrm{in}}]^{+}_{\mathbf{g}'i'}\exp\left[\mathrm{i}\mathbf{K}^{+}_{\mathbf{g}'}\cdot(\mathbf{r}-\mathbf{A}_{\mathrm{L}})\right]\widehat{\mathbf{e}}_{i'}$, incident on the slab from the left, we finally obtain a reflected wave $\sum_{\mathbf{g}i}[E_{\mathrm{rf}}]^{-}_{\mathbf{g}i}\exp\left[\mathrm{i}\mathbf{K}^{+}_{\mathbf{g}}\cdot(\mathbf{r}-\mathbf{A}_{\mathrm{L}})\right]\widehat{\mathbf{e}}_{i}$ on the left of the slab and a transmitted wave $\sum_{\mathbf{g}i}[E_{\mathrm{tr}}]^{+}_{\mathbf{g}i}\exp\left[\mathrm{i}\mathbf{K}^{+}_{\mathbf{g}}\cdot(\mathbf{r}-\mathbf{A}_{\mathrm{R}})\right]\widehat{\mathbf{e}}_{i}$ on the right of the slab, where $\mathbf{A}_{\mathrm{L}}$ ($\mathbf{A}_{\mathrm{R}}$) is the appropriate origin at the left (right) interface of the entire slab. We have

$$[E_{\mathrm{tr}}]^{+}_{\mathbf{g}i}=Q^{\mathrm{I}}_{\mathbf{g}i;\mathbf{g}'i'}\,[E_{\mathrm{in}}]^{+}_{\mathbf{g}'i'}\quad\text{and}\quad[E_{\mathrm{rf}}]^{-}_{\mathbf{g}i}=Q^{\mathrm{III}}_{\mathbf{g}i;\mathbf{g}'i'}\,[E_{\mathrm{in}}]^{+}_{\mathbf{g}'i'}\ , \tag{10}$$

where $\mathbf{Q}^{\mathrm{I}}$, $\mathbf{Q}^{\mathrm{III}}$ are the appropriate transmission and reflection matrices of the slab. After calculating the transmitted and reflected waves on the right and left of the slab, we can obtain the corresponding transmittance $\mathcal{T}(\omega,\mathbf{k}_{\|}+\mathbf{g}',i')$ and reflectance $\mathcal{R}(\omega,\mathbf{k}_{\|}+\mathbf{g}',i')$ of the slab. These are defined as the ratio of the transmitted, respectively the reflected, energy flux to the energy flux associated with the incident wave. We obtain

$$\mathcal{T}=\frac{\sum_{\mathbf{g}i}\left|[E_{\mathrm{tr}}]^{+}_{\mathbf{g}i}\right|^{2}K^{+}_{\mathbf{g}z}}{\left|[E_{\mathrm{in}}]^{+}_{\mathbf{g}'i'}\right|^{2}K^{+}_{\mathbf{g}'z}}\quad\text{and}\quad\mathcal{R}=\frac{\sum_{\mathbf{g}i}\left|[E_{\mathrm{rf}}]^{-}_{\mathbf{g}i}\right|^{2}K^{+}_{\mathbf{g}z}}{\left|[E_{\mathrm{in}}]^{+}_{\mathbf{g}'i'}\right|^{2}K^{+}_{\mathbf{g}'z}}\,. \tag{11}$$

We remember that only propagating beams (those with $K^+_{\mathbf{g}z}$ real) enter the numerators of the above equations. Finally we note that if absorption is present it can be calculated from the requirement of energy conservation:

$$\mathcal{A} = 1 - \mathcal{T} - \mathcal{R}. \tag{12}$$

Here we have tacitly assumed that the same host medium extends to the left and right of the slab to infinity, but the extension of the formalism to allow for different materials on both sides of the slab is straightforward.[3,4]

The S matrix is defined, in general terms, as the matrix which transforms the incoming wave field into the outgoing wave field, and in the plane-wave representation is given by

$$\begin{aligned}
S^{++}_{\mathbf{g}i;\mathbf{g}'i'} &= \exp\left[-\mathrm{i}\left(\mathbf{K}^+_{\mathbf{g}}\cdot\mathbf{A}_{\mathrm{R}} - \mathbf{K}^+_{\mathbf{g}'}\cdot\mathbf{A}_{\mathrm{L}}\right)\right] Q^{\mathrm{I}}_{\mathbf{g}i;\mathbf{g}'i'} \\
S^{+-}_{\mathbf{g}i;\mathbf{g}'i'} &= \exp\left[-\mathrm{i}\left(\mathbf{K}^+_{\mathbf{g}}\cdot\mathbf{A}_{\mathrm{R}} - \mathbf{K}^-_{\mathbf{g}'}\cdot\mathbf{A}_{\mathrm{R}}\right)\right] Q^{\mathrm{II}}_{\mathbf{g}i;\mathbf{g}'i'} \\
S^{-+}_{\mathbf{g}i;\mathbf{g}'i'} &= \exp\left[-\mathrm{i}\left(\mathbf{K}^-_{\mathbf{g}}\cdot\mathbf{A}_{\mathrm{L}} - \mathbf{K}^+_{\mathbf{g}'}\cdot\mathbf{A}_{\mathrm{L}}\right)\right] Q^{\mathrm{III}}_{\mathbf{g}i;\mathbf{g}'i'} \\
S^{--}_{\mathbf{g}i;\mathbf{g}'i'} &= \exp\left[-\mathrm{i}\left(\mathbf{K}^-_{\mathbf{g}}\cdot\mathbf{A}_{\mathrm{L}} - \mathbf{K}^-_{\mathbf{g}'}\cdot\mathbf{A}_{\mathrm{R}}\right)\right] Q^{\mathrm{IV}}_{\mathbf{g}i;\mathbf{g}'i'}
\end{aligned} \tag{13}$$

for the given ω and $\mathbf{k}_\parallel$. The phase factors in Eq. (13) arise from the need to refer all waves to a common origin. The S matrix is a unitary matrix because of flux conservation, and causality condition implies that its eigenvalues are analytic functions in the upper complex frequency half-plane but they may have poles in the lower half-plane at $\omega_i - \mathrm{i}\gamma_i$, $\gamma_i \geq 0$; ω_i is the eigenfrequency while γ_i denotes the inverse of the lifetime of the respective mode. Solutions with $\gamma_i/\omega_i \ll 1$ correspond to resonant modes and are of particular physical interest. The eigenfrequencies of possible bound states can be obtained, separately, from the condition for the existence of a wave field localized within the slab. Dividing the slab into a left and a right part, with respect to the localization region, this condition leads to the secular equation: $\det[\mathbf{I} - \mathbf{Q}^{\mathrm{II}}_{\mathrm{left}}\mathbf{Q}^{\mathrm{III}}_{\mathrm{right}}] = 0$.

We first apply the extended layer-multiple-scattering method to study the plasmonic excitations of square arrays of gold-silica-gold nanosandwiches on a quartz substrate ($\epsilon_{\mathrm{quartz}} = 2.13$, $\mu_{\mathrm{quartz}} = 1$). A periodic array of nanosandwiches is built of consecutive layers of appropriate nanodisks, through the proper combination of the Q matrices of the component layers. For the dielectric function of gold we interpolate to the bulk values measured by Johnson and Christy[7] and for silica we assume a dielectric constant of 2.13. In order to ensure adequate convergence in our calculations, we truncate the spherical-wave expansions at $\ell_{\max} = 13$ and take into account 137 $\mathbf{g}$ vectors in the relevant plane-wave expansions, while the scattering T matrix of the single nanodisk is calculated with $\ell_{\mathrm{cut}} = 16$ and a Gaussian quadrature integration formula with 4000 points.[5] We consider nanosandwiches of diameter d =100 nm and typical thickness h_1=20 nm gold, h_2=20 nm silica and h_3=20 nm gold, arranged on a square lattice with lattice constant a =300 nm. Such large interparticle separations essentially correspond to isolated particles as we discuss below. In order to study the hybridization between the particle plasmons of the two metallic nanodisks, we keep their thickness fixed ($h_1 = h_3$=20 nm) and vary the thickness h_2 of the dielectric spacer. Corresponding extinction spectra (extinction=negative logarithm of the transmittance) at normal incidence are depicted in the middle panel of Fig. 3. It can be seen that, for very thin dielectric spacers, we obtain a single peak, which is essentially the single particle plasmon resonance in the corresponding array of simple gold disks 40 nm-thick (see upper panel of Fig. 3). On the other hand, when the separation between gold disks in the nanosandwich is large enough and consequently their interaction is small, the extinction spectrum tends to that of the corresponding array of simple gold disks 20 nm-thick. For intermediate thickness of the dielectric spacer the spectra exhibit two distinct peaks. The high-frequency (short-wavelength) peak shifts to the red with increasing thickness of the dielectric spacer, while the low-frequency (long-wavelength) peak shifts to the blue and gradually becomes more probounced as the thickness of the spacer increases. These results can be understood as follows. The optical response of the single gold nanodisk is dominated by a particle plasmon resonance which is predominantly of dipole electric type. The interaction between these modes of the constituent gold nanodisks in the nanosandwich results into a symmetric high-frequency hybrid mode (the electric field oscillates in phase in the two gold nanodisks normal to their axis) and an antisymmetric low-frequency hybrid mode (the electric field oscillates with opposite phase in the two gold nanodisks normal to their axis). The double-peak structure in the calculated extinction spectra results from the excitation of theses

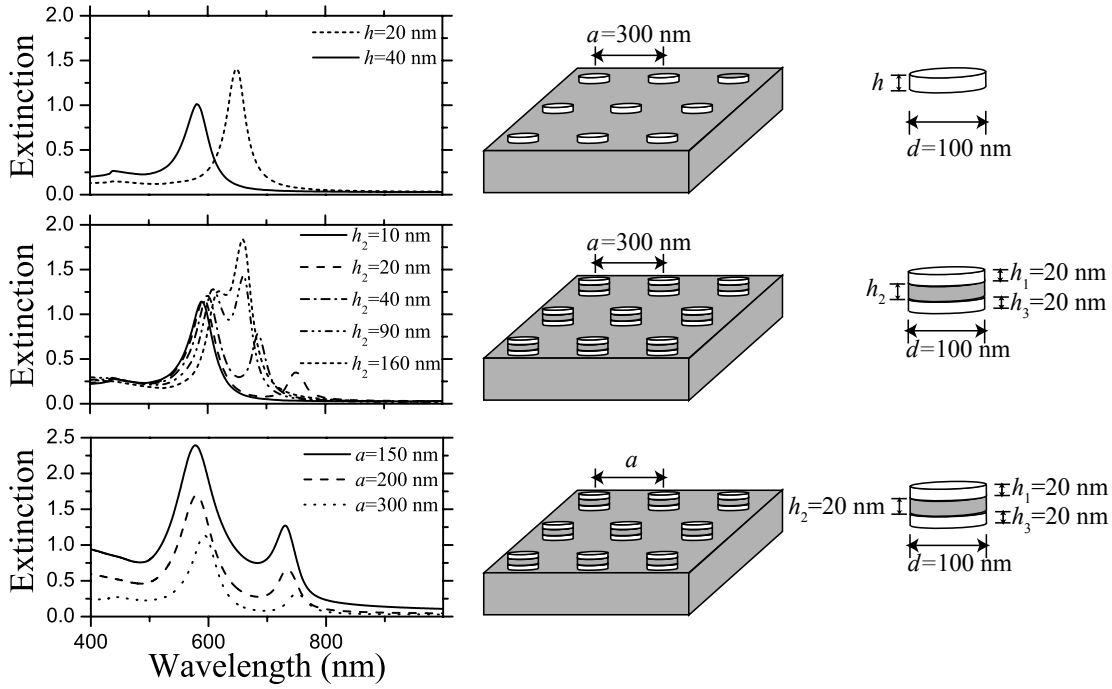

Figure 3. Upper panel: Extinction at normal incidence of a square array, with lattice constant a =300 nm, of gold disks with diameter d =100 nm and thickness h = 40 nm and h = 20 nm, on a quartz substrate. Middle panel: Extinction at normal incidence of square arrays, with lattice constant a =300 nm, of gold-silica-gold nanosandwiches with diameter d =100 nm. The gold disks have a thickness $h_1 = h_3 = 20$ nm and the different spectra correspond to thickness of the silica spacer, h_2, varying from 10 to 160 nm. Lower panel: Extinction at normal incidence of square arrays of gold-silica-gold nanosandwiches, with $h_1 = h_2 = h_3 = 20$ nm and diameter d =100 nm, on a quartz substrate. The different spectra correspond to lattice constants, a, varying from 150 to 300 nm.

modes. Interestingly, when the separation between gold disks is small (<10 nm) the low-frequency peak is not observed. Our results are in good agreement with existing experimental data on isolated nanosandwiches.[9,10] The interaction between nanosandwiches increases as we reduce the lattice constant and is manifested as a small shift of the resonance peaks and more pronounced extinction, as can be seen in the lower panel of Fig. 3.

We shall now study the optical response of a 2D periodic array of metallic nanodisks on top of an indium tin oxide (ITO) film, on a quartz substrate. An ITO film ($\epsilon_{\rm ITO} = 3.6$, $\mu_{\rm ITO} = 1$) on a quartz substrate ($\epsilon_{\rm quartz} = 2.13$, $\mu_{\rm quartz} = 1$) supports waveguide modes of the EM field. Along any direction parallel to the interfaces these modes have the form of propagating waves with a wave vector $\mathbf{q}_{\|}$; along the normal direction they decay exponentially to zero away from the film on either side of it. There are transverse electric (TE) guided modes (the electric field oscillates parallel to the interfaces) and transverse magnetic (TM) guided modes (the magnetic field oscillates parallel to the interfaces). These modes lie outside the light cone in the surrounding media and, therefore, cannot be excited by an externally incident wave. They cannot match continuously a propagating mode of the EM field outside the film; momentum and energy cannot be conserved simultaneously. The presence of a 2D periodic array of particles on the film transforms waveguide modes from bound to radiative through an umklapp process: a plane wave of wave number q, incident on the periodic array, generates a number of diffracted beams with wave vectors $\mathbf{K}_{\mathbf{g}}^{\pm} = \mathbf{k}_{\|} + \mathbf{g} \pm \sqrt{q^2 - (\mathbf{k}_{\|} + \mathbf{g})^2}\widehat{\mathbf{e}}_z$. If $q < |\mathbf{k}_{\|} + \mathbf{g}|$ we obtain evanescent diffracted beams which can match continuously the corresponding guided waves of the same polarization and of the same $\mathbf{q}_{\|} = \mathbf{k}_{\|} + \mathbf{g}$, provided they have the right frequency. Accordingly, the waveguide modes are no longer bound within the film, but leak into the outer region becoming resonant states. These modes can be excited by an externally incident wave and manifest themselves as resonance structures in the transmission spectrum. From another point of view, because of the 2D periodicity of the coating layer, the waveguide frequency bands are folded within the SBZ of the given lattice and acquire a small imaginary part due to the mixing with the

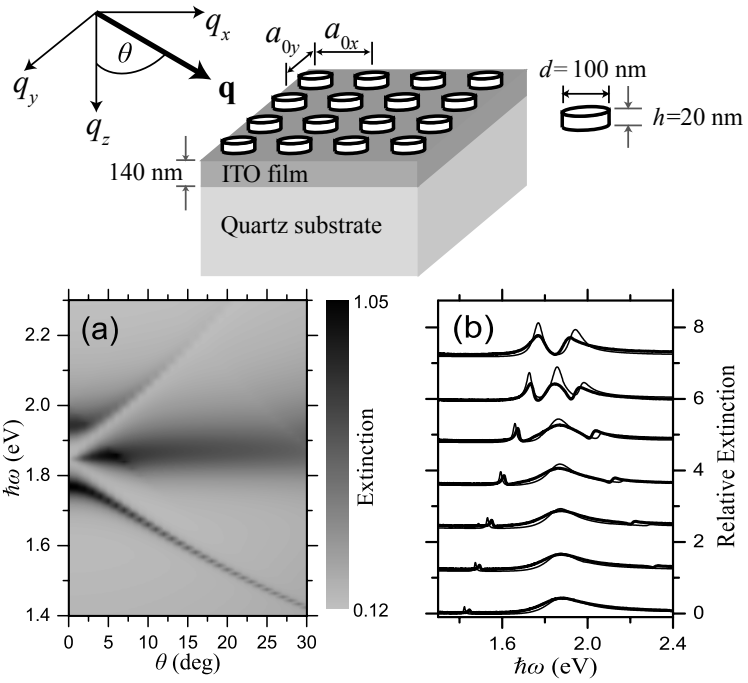

Figure 4. A rectangular array ($a_{0x} = 425$ nm, $a_{0y} = 300$ nm) of gold nanodisks ($d = 100$ nm, $h = 20$ nm) on top of an ITO film, 140 nm-thick, on a quartz substrate. Light is incident in the xz plane at an angle θ and polarization along the y direction. (a): Theoretical extinction as a function of frequency and the angle of incidence. (b): Experimental[11] (thick lines) and theoretical (thin lines) relative extinction of the system with respect to the uncoated ITO film on the quartz substrate. The different spectra are shifted upwards for clarity and correspond, from top to bottom, to θ varying from 0^o to 30^o with a step of 5^o.

extended (scattering) states.

Let us consider an ITO film, 140 nm-thick, on a semi-infinite quartz substrate, coated with a rectangular array, defined by the primitive vectors $\mathbf{a}_1 = (a_{0x}, 0, 0)$ and $\mathbf{a}_2 = (0, a_{0y}, 0)$ with lattice constants $a_{0x} = 425$ nm and $a_{0y} = 300$ nm, of gold nanodisks ($d = 100$ nm, $h = 20$ nm). The structure under consideration is shown in the upper panel of Fig. 4. The weak interaction between the fundamental dipole-like plasmon modes of the periodically arranged nanodisks removes the twofold degeneracy of this mode of the single nanodisk and two relatively flat bands of collective particle-plasmon states are formed. These bands are superimposed to those of the bare waveguide to give the 2D band diagram of resonant states of the 3D composite system. These states, which have a relatively long lifetime (their eigenfrequency has a small imaginary part), can be excited, in general, by an externally incident wave and manifest themselves as pronounced peaks in the reflection and absorption spectra. Bands of the same symmetry interact and repel each other. This mechanism removes, for instance, the degeneracy of the waveguide modes at the edges and the center of the SBZ (Bragg gaps). The same mechanism also leads to a hybridization between particle-plasmon and waveguide bands. In the system under consideration, the bands are classified as odd or even, if the electric field associated with the corresponding eigenmodes is odd or even upon reflection with respect to the xz plane, respectively. The dispersion diagram of the odd modes can be probed through the extinction spectra for light incident at an angle in the xz plane and polarization along the y direction (s polarization). As shown in Fig. 4(a), in this case, two odd (TE) waveguide modes and one odd particle-plasmon mode are excited. Similarly, p-polarized light (polarization in the xz plane) can probe the even modes. It is worthnoting that the presence of the film and the substrate induces a considerable red shift of the particle-plasmon modes, as can be seen by comparing Figs. 1(c) and 4.

In Fig. 4(b) we compare our results with available experimental data.[11] This figure depicts the relative extinction of the system with respect to the uncoated ITO film on the quartz substrate, i.e., the quantity $-\ln(\mathcal{T}/\mathcal{T}_0)$ where $\mathcal{T}$ ($\mathcal{T}_0$) is the transmittance of the quartz-ITO-air system with (without) the coating layer of

nanodisks, for different angles of incidence. In order to obtain good quantitative agreement between experiment and theory as far as the peak positions are concerned, we need to shift the nanodisk array by 3 nm away from the ITO film. We note that a small separation of the nanodisks from the ITO film may also exist in the lithographically fabricated samples, e.g., due to the presence of a buffer layer. Our calculations were carried out using the experimental dielectric function of bulk gold,[7] including a finite-size correction. In the case of a small metallic particle, the electronic mean free path is shorter than in the bulk metal and this effect can be incorporated by adding a size-dependent correction $\Delta\epsilon = \omega_{\rm p}^2[(\omega^2 + {\rm i}\omega\tau^{-1})^{-1} - (\omega^2 + {\rm i}\omega\tau_{\rm s}^{-1})^{-1}]$ to the bulk dielectric function, where $\tau_{\rm s}^{-1} = \tau^{-1} + v_{\rm F} L_{\rm eff}^{-1}$ is the inverse relaxation time corrected for the finite size of the particle; $v_{\rm F}$ is the Fermi velocity in the bulk material and $L_{\rm eff}$ an effective linear dimension of the particle.[12] We have taken this finite-size correction into account using the values $\hbar\omega_{\rm p} = 9$ eV, $\hbar\tau^{-1} = 0.06$ eV, $\hbar v_{\rm F} = 0.9$ eV nm which are appropriate for gold[6,7] and $L_{\rm eff} = 30$ nm as an effective linear dimension of the nanodisk.[12] In order to ensure adequate convergence, here, we need to truncate the angular-momentum expansions at $\ell_{\max} = 12$ and take into account 161 $\mathbf{g}$ vectors in the relevant plane-wave expansions, while the T matrix is calculated with $\ell_{\rm cut} = 16$ and a Gaussian quadrature integration formula with 4000 points.[5] It can be seen that our theoretical results are in excellent agreement with the experimental data. The fact that particle-plasmon resonances appear, in general, sharper in the theoretical than in the experimental spectra is likely to be ascribed to fabrication imperfections in particle shape, size and arrangement.

4. PHOTONIC BAND STRUCTURE OF A SIMPLE CUBIC CRYSTAL OF METALLIC NANODISKS

Within the layer-multiple-scattering method, an infinite 3D crystal is viewed as a sequence of identical slabs parallel to the xy plane (a given crystallographic plane), extending over all space from $z = -\infty$ to $z = +\infty$. The unit slab may consist of a single layer or any number of layers, provided they have the same 2D periodicity, specified by the primitive lattice vectors $\mathbf{a}_1$, $\mathbf{a}_2$. If $\mathbf{a}_3$ is a vector which takes us from a point in the $n_{\rm L}$th slab to an equivalent point in the $(n_{\rm L}+1)$th slab, then $\{\mathbf{a}_1, \mathbf{a}_2, \mathbf{a}_3\}$ is a set of primitive vectors for the crystal.

In the host region between the $n_{\rm L}$th and the $(n_{\rm L}+1)$th slabs the electric field, of given ω and $\mathbf{k}_\parallel$, has the form

$$\mathbf{E}(\mathbf{r}) = \sum_{\mathbf{g}i} \left\{ E_{\mathbf{g}i}^{+}(n_{\rm L}) \exp\left[{\rm i}\mathbf{K}_{\mathbf{g}}^{+} \cdot \left(\mathbf{r} - \mathbf{A}(n_{\rm L})\right)\right] + E_{\mathbf{g}i}^{-}(n_{\rm L}) \exp\left[{\rm i}\mathbf{K}_{\mathbf{g}}^{-} \cdot \left(\mathbf{r} - \mathbf{A}(n_{\rm L})\right)\right] \right\} \widehat{\mathbf{e}}_i, \tag{14}$$

where $\mathbf{A}(n_{\rm L})$ is the appropriate origin between the $n_{\rm L}$th and $(n_{\rm L}+1)$th slabs.

A generalized Bloch wave, by definition, has the property

$$E_{\mathbf{g}i}^{s}(n_{\rm L}+1) = \exp\left({\rm i}\mathbf{k}\cdot\mathbf{a}_3\right) E_{\mathbf{g}i}^{s}(n_{\rm L}), \tag{15}$$

with $\mathbf{k} = \left(\mathbf{k}_\parallel, k_z(\omega, \mathbf{k}_\parallel)\right)$, where k_z is, for a given $\mathbf{k}_\parallel$, a function of ω, to be determined. The reduced zone of the 3D $\mathbf{k}$ space is chosen as follows: $(\mathbf{k}_\parallel, k_z)$ where $\mathbf{k}_\parallel = (k_x, k_y)$ extends over the SBZ of the given crystallographic plane, and $-|\mathbf{b}_3|/2 < {\rm Re}[k_z] \le |\mathbf{b}_3|/2$, where $\mathbf{b}_3 \equiv 2\pi\mathbf{a}_1 \times \mathbf{a}_2 / \mathbf{a}_1 \cdot (\mathbf{a}_2 \times \mathbf{a}_3) = \widehat{\mathbf{e}}_z 2\pi/a_{3z}$. This reduced $\mathbf{k}$ zone is of course completely equivalent to the commonly used, more symmetrical bulk Brillouin zone, in the sense that a point in one of them lies also in the other or differs from such one by a vector of the 3D reciprocal lattice.

The coefficients $E_{\mathbf{g}i}^{s}(n_{\rm L})$ are obviously related to the $E_{\mathbf{g}i}^{s}(n_{\rm L}+1)$ coefficients through the Q matrices of the unit slab; these relations taken together with Eq. (15) lead to the following system of equations

$$\begin{bmatrix} \mathbf{Q}^{\rm I} & \mathbf{Q}^{\rm II} \\ -\left[\mathbf{Q}^{\rm IV}\right]^{-1}\mathbf{Q}^{\rm III}\mathbf{Q}^{\rm I} & \left[\mathbf{Q}^{\rm IV}\right]^{-1}\left[\mathbf{I} - \mathbf{Q}^{\rm III}\mathbf{Q}^{\rm II}\right] \end{bmatrix} \begin{bmatrix} \mathbf{E}^{+}(n_{\rm L}) \\ \mathbf{E}^{-}(n_{\rm L}+1) \end{bmatrix} = \exp\left({\rm i}\mathbf{k}\cdot\mathbf{a}_3\right) \begin{bmatrix} \mathbf{E}^{+}(n_{\rm L}) \\ \mathbf{E}^{-}(n_{\rm L}+1) \end{bmatrix}, \tag{16}$$

where $\mathbf{E}^{\pm}$ are the appropriate column matrices. In practice we keep $g_{\max}$ reciprocal-lattice vectors (those of the smallest magnitude) in which case $\mathbf{E}^{\pm}$ are column matrices with $2g_{\max}$ elements.

For given ω and $\mathbf{k}_\parallel$, we obtain the eigenvalues of k_z from the eigenvalues of the matrix on the left-hand side of Eq. (16). The eigenvalues of $k_z(\omega, \mathbf{k}_\parallel)$, looked upon as functions of real ω, define, for each $\mathbf{k}_\parallel$, lines (sometimes they are called real-frequency lines) in the complex k_z plane. Taken together they constitute the complex band

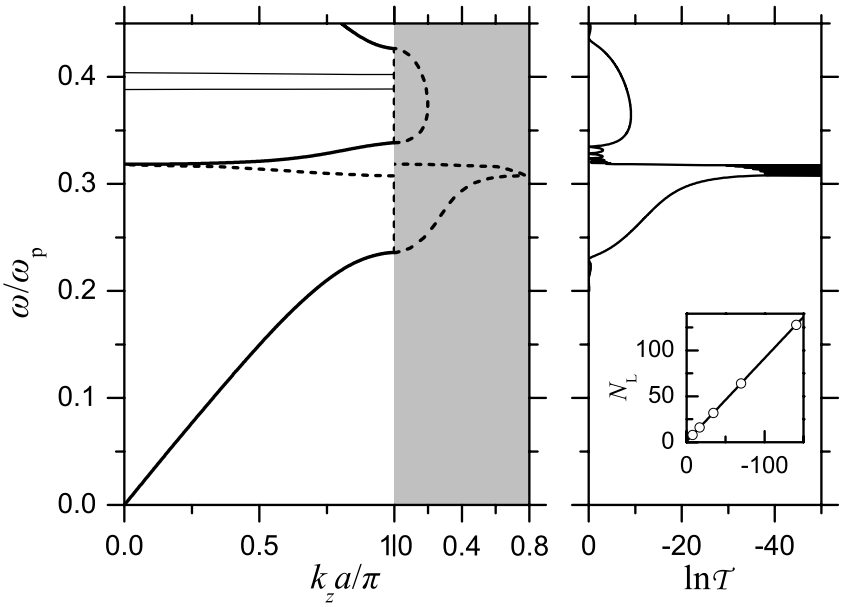

Figure 5. Left-hand diagram: The photonic band structure of a sc crystal, with lattice constant $a = 9c/\omega_p$, of nanodisks ($d = 5c/\omega_p,\ h = c/\omega_p$) made of a nonabsorbing Drude metal, in air, along the [001] direction. The thick and thin lines denote the doubly degenerate and nondegenerate bands, respectively. In the gap regions we show by dashed lines the doubly degenerate real-frequency lines with the smallest imaginary part of k_z (plotted in the shaded area). Right-hand diagram: Transmittance (in logarithmic scale) at normal incidence of a slab of $N_L = 8$ (001) planes of the above crystal. The inset depicts the transmittance at a given frequency $\omega = 0.25\omega_p$ within the gap as a function of the thickness of the slab.

structure of the infinite crystal associated with the given crystallographic plane. A line of given $\mathbf{k}_\parallel$ may be real (in the sense that k_z is real) over certain frequency regions, and be complex (in the sense that k_z is complex) for ω outside these regions. It turns out that for given $\mathbf{k}_\parallel$ and ω, out of the eigenvalues of $k_z(\omega, \mathbf{k}_\parallel)$ none or, at best, a few are real; the eigenvectors of Eq. (16), corresponding to them, represent propagating modes of the EM field in the given infinite crystal. The remaining eigenvalues of $k_z(\omega, \mathbf{k}_\parallel)$ are complex and the corresponding eigenvectors represent evanescent waves. These have an amplitude which increases exponentially in the positive or negative z direction and, unlike the propagating waves, do not exist as physical entities in the infinite crystal. However, they are an essential part of the physical solutions of the EM field in a slab of finite thickness. A region of frequency where propagating waves do not exist, for given $\mathbf{k}_\parallel$, constitutes a frequency gap of the EM field for the given $\mathbf{k}_\parallel$. If over a frequency region no propagating wave exists whatever the value of $\mathbf{k}_\parallel$, then this region constitutes an absolute frequency gap. Finally, it is worth noting that, when for a given value of $\mathbf{k}_\parallel$ there is a symmetry operation of the crystal which transforms $(\mathbf{k}_\parallel, k_z)$ to $(\mathbf{k}_\parallel, -k_z)$, the eigensolutions (Bloch waves) of Eq. (16) appear in pairs: $k_z(\omega, \mathbf{k}_\parallel)$ and $-k_z(\omega, \mathbf{k}_\parallel)$.

As an example of a 3D photonic crystal, we consider a simple cubic structure, with lattice constant $a = 9c/\omega_p$, of metallic nanodisks described by the Drude dielectric function, with dimensions $d = 5c/\omega_p$ and $h = c/\omega_p$, in air, and view the crystal as a sequence of (001) planes of particles. We deliberately disregard absorption in the metallic material, taking $\tau^{-1} = 0$ in Eq. (1), in order to be able to calculate the frequency band structure in an unambiguous manner. In the numerical calculations we consider $\ell_{max} = 10$ and 37 $\mathbf{g}$ vectors while the T matrix is evaluated with $\ell_{cut} = 14$ and 2000 points for the Gaussian integration, in order to ensure adequate convergence. In the left-hand panel of Fig. 5 we show the photonic band structure of this crystal along the [001] direction, i.e., for $\mathbf{k}_\parallel = \mathbf{0}$. We note that the (001) surface of the crystal under consideration is a plane of mirror symmetry and, therefore, the frequency bands appear in pairs: $k_z(\omega, \mathbf{k}_\parallel)$ and $-k_z(\omega, \mathbf{k}_\parallel)$; for this reason, in this figure we show the bands only for positive k_z. Along the [001] direction, the bands are either nondegenerate or doubly degenerate. While the doubly degenerate bands can be excited by an externally incident wave, the

nondegenerate bands cannot, because they do not have the proper symmetry.

At low frequencies we obtain a doubly degenerate linear dispersion curve, as expected for propagation in a homogeneous medium characterized by a frequency-independent effective refractive index. This extended effective-medium band is folded within the first Brillouin zone (BZ) and a relatively wide Bragg gap opens up at the BZ boundary. In addition, flat bands are formed from the particle-plasmon modes of the individual nanodisks that interact weakly between them. Along the [001] direction, in the frequency region under consideration, there is one doubly degenerate flat band within the gap, which originates from the fundamental dipole-like particle-plasmon modes. Moreover, the lowest quadrupole-like particle-plasmon modes give rise to two nondegenerate flat bands in the gap, about $0.389\omega_{\rm p}$ and $0.403\omega_{\rm p}$.

The right-hand panel of Fig. 5 displays the transmittance of a slab of the crystal under consideration consisting of $N_{\rm L} = 8$ (001) planes of nanodisks. In the frequency region of the extended effective-medium band, the transmittance is about unity and exhibits the well-known Fabry-Perot oscillations due to multiple scattering between the surfaces of the slab. The period of these oscillations, which are not discernible in the logarithmic scale of the figure, corresponds to $k_z a/\pi = 1/8$, as expected for the given slab thickness. Within the gap region the transmission coefficient practically vanishes, except in the short frequency range of the flat doubly degenerate band where resonant transmission takes place.

In the left-hand panel of Fig. 5, apart from the ordinary frequency bands (k_z is real), we also show the real-frequency lines for complex eigenvalues k_z that correspond to the doubly degenerate bands. These lines are the analytic continuations in the complex k_z plane of the bands below and above the gaps. The real-frequency line of the appropriate symmetry (doubly degenerate in the present case) with the smallest imaginary part over a frequency gap determines the attenuation of the wave field over this region; we obtain $\ln \mathcal{T}(\omega) = -2aN_{\rm L}{\rm Im}[k_z(\omega)] + {\rm const.}$, for a given value of $\mathbf{k}_\parallel$. This is indeed observed in the right-hand panel of Fig. 5. The inset of this figure depicts the logarithm of the transmittance at a given frequency $\omega = 0.25\omega_{\rm p}$ within the first gap as a function of the thickness of the slab (open circles). The straight line has a slope equal to $-2a0.176\pi/a$, where $0.176\pi/a$ is the smallest imaginary part of $k_z(0.25\omega_{\rm p}, \mathbf{k}_\parallel = \mathbf{0})$.

5. CONCLUSION

In summary, we reported on the optical response of plasmonic systems of 2D and 3D ordered arrays of metallic nanodisks by means of full electrodynamic calculations using the extended layer-multiple-scattering method and showed that the method retains its high efficiency and accuracy even in cases of particles with edges and strong deviation from the spherical shape. Starting from a detailed analysis of the particle-plasmon modes of single metallic nanocylinders of different aspect ratios, we investigated square arrays of gold-silica-gold nanosandwiches on a quartz substrate and showed that plasmon hybridization leads to a double-peak structure in the extinction spectrum, with a symmetric and an antisymmetric resonance. Our results corroborate that such structures, with a tailored optical response, can be useful for practical applications, e.g., as chemical and biological sensors, while the presence of an antisymmetric resonance makes metallodielectric nanosandwiches potential candidates as building units in the design of novel negative-index metamaterials. Moreover, we studied the interaction between waveguide modes of an ITO film on a quartz substrate and collective plasmonic modes of a rectangular periodic overlayer of gold nanodisks. Our results are in very good quantitative agreement with available experimental data and provide a consistent interpretation of the underlying physics. Finally, we studied a simple cubic photonic crystal of metallic nanodisks; we analyzed transmission spectra of finite slabs of this crystal by reference to relevant complex-band diagrams and demonstrated the physical origin of the field eigenmodes.

ACKNOWLEDGMENTS

This work was supported by NCSR "Demokritos" under "Demoerevna" E-1437 and by the research programme "Kapodistrias" of the University of Athens.

REFERENCES

1. Ozbay, E., "Plasmonics: Merging photonics and electronics at nanoscale dimensions," Science 311(5758), 189-193 (2006).
2. García de Abajo, F. J., "Colloquium: Light scattering by particle and hole arrays," Rev. Mod. Phys. 79(4), 1267-1290 (2007).
3. Stefanou, N., Yannopapas, V. and Modinos, A., "Heterostructures of photonic crystals: Frequency bands and transmission coefficients," Comput. Phys. Commun. 113(1), 49-77 (1998).
4. Stefanou, N., Yannopapas, V. and Modinos, A., "MULTEM 2: A new version of the program for transmission and band structure calculations of photonic crystals," Comput. Phys. Commun. 132(1-2), 189-196 (2000).
5. Gantzounis, G. and Stefanou, N., "Layer-multiple-scattering method for photonic crystals of nonspherical particles," Phys. Rev. B 73(3), art. no. 035115 (2006).
6. Ashcroft, N. W. and Mermin, N. D., [Solid State Physics], Saunders, New York (1976).
7. Johnson, P. B. and Christy, R. W., "Optical constants of the noble metals," Phys. Rev. B 6(12), 4370-4379 (1972).
8. Novotny, L., "Effective wavelength scaling for optical antennas," Phys. Rev. Lett. 98(26), art. no. 266802 (2007).
9. Su, K. H., Wei, Q. H. and Zhang, X., "Tunable and augmented plasmon resonances of $Au/SiO_2/Au$ nanodisks," Appl. Phys. Lett. 88(6), art. no. 063118 (2006).
10. Dmitriev, A., Pakizeh, T., Käll, M. and Sutherland, D. S., "Gold-silica-gold nanosandwiches: Tunable bimodal plasmonic resonators," Small 3(2), 294-299 (2007).
11. Christ, A., Linden, S., Zentgraf, T., Nau, D., Tikhodeev, S. G., Gippius, N. A., Kuhl, J., Schindler, F., Holleitner, A. W., Stehr, J., Crewett, J., Lupton, J., Klar, T., Scherf, U., Feldmann, J., Dahmen, C., von Plessen, G. and Giessen, H., "Optical properties of planar metallodielectric photonic crystals" in [Photonic Crystals: Advances in Design, Fabrication, and Characterization], Busch, K., Lölkes, S., Wehrspohn, R. B. and Föll, H. eds., 85-108, Wiley, New York (2004).
12. Coronado, E. A. and Schatz, G. C., "Surface plasmon broadening for arbitrary shape nanoparticles: A geometrical probability approach," J. Chem. Phys. 119(7), 3926-3934 (2003).